Journal of the Korean Ceramic Society
Vol. 43, No. 8, pp. 472~478, 2006.

The Effect of Processing Variables and Composition on the Nitridation Behavior of Silicon Powder Compact

Young-Jo Park,† Hyung-Woo Lim, Eugene Choi, and Hai-Doo Kim

Powder Materials Research Center, Korea Institute of Machinery and Materials, Changwon 641-010, Korea
(Received July 3, 2006; Accepted August 15, 2006)

ABSTRACT

The effect of compositional and processing variables on a nitriding reaction of silicon powder compact and subsequent post sintering of RBSN (Reaction-Bonded Silicon Nitride) was investigated. The addition of a nitriding agent enhanced nitridation rate substantially at low temperatures, while the formation of a liquid phase between the nitriding agent and the sintering additives at a high temperature caused a negative catalyst effect resulting in a decreased nitridation rate. A liquid phase formed by solely an additive, however, was found to have no effect on nitridation for the additive amount used in this research. The original site of a decomposing pore former was loosely filled by a reaction product (Si_3N_4), which provided a specimen with nitriding gas passage. For SRBSN (Sintered RBSN) specimens of high porosity, only a marginal dimensional change was measured after post sintering. Its engineering implication for near-net shaping ability is discussed.

Key words : RBSN, SRBSN, Nitridation rate, Porosity, DPF

1. Introduction

Since the early 1990's in the area of Si_3N_4 ceramics, there have been certain research activities that have diverted from conventional structural applications. Particularly owing to such planned usages as a substrate in devices,[1-6] machinable ceramics,[7,8] and filtering media,[9-12] technological investigations of Si_3N_4 ceramics have mainly concentrated on the enhancement of their thermal conductivity and the development of porous bodies with a controlled microstructure, e.g. grain morphology and pore size distribution.

Much attention has been paid to the thermal conductivity of Si_3N_4 ceramics from the time when Haggerty and Lightfoot[13] pointed out that Si_3N_4 is a potential high thermal conductive material with an intrinsic thermal conductivity of 200-300 W/mK at room temperature. A significant increase in the thermal conductivity, more than 140 W/mK compared to about 20 W/mK for typical applications, has been achieved through the use of high purity raw powders with effective sintering additives.[4,5] These facts combined with the superior mechanical properties of Si_3N_4 ceramics are expected to open up new applications for Si_3N_4 ceramics as a high-temperature substrate in high-powerd electrical devices. In addition, the improved thermal conductivity is also very important for application in automotive engines, where good thermal shock resistance is required.

†Corresponding author : Young-Jo Park
E-mail : yjpark87@kmail.kimm.re.kr
Tel : +82-55-280-3356 Fax : +82-55-280-3392

One of the significant disadvantages of engineering ceramics is their difficulty in machining after sintering, which leads to high machining cost keeping them from wider usages. To address this, various ceramics having good machinability known as machinable ceramics have been developed, and porous Si_3N_4 material is one option pursued.[7,8] Recent studies suggest that the presence of pores can improve the performance with a carefully controlled microstructure.[14,15] By adjusting the characteristics of the sintering additives, such as the type and amount, porous Si_3N_4 ceramics have been developed through the same sintering process used to obtain dense Si_3N_4 ceramics. Thus, the acquired porous Si_3N_4 ceramics not only have machinability, but with textured rod-like β-Si_3N_4 grains show the superior mechanical properties of a high strength, good thermal shock resistance, and high strain and damage tolerance.

In addition to providing machinability, porous ceramic materials have many industrial applications as filtering media, including high-temperature gas filters, separation membranes, and catalyst supports. There have been restricted efforts to replace the currently commercialized Cordierite, a SiC honeycomb filter in a Diesel Particulate Filter (DPF), with Si_3N_4 ceramics.[9] A DPF is a component that traps and eliminates Particulate Matters (PM) contained in the exhaust gas of diesel-powered vehicles. Diesel vehicles are both economic and environmentally friendly due to their higher heat efficiency of greater than 20% and their lower emission of earth-warming CO_2 of less than 90%, as compared with gasoline vehicles. In spite of these positive factors, diesel vehicles have their own problems.

For example, their exhaust contains a relatively large amount of NOx and PM. In advanced countries, the attachment of a DPF on diesel vehicles is required by law. Recently in Europe, the market share of diesel vehicles among newly built passenger cars has approached nearly 50 percent, and this rate continues to increase. As a DPF gradually clogs with PM with continuous use, the filter needs to be regenerated by combusting the accumulated PM. A cordierite filter is inferior in terms of durability due to its low melting point and low corrosion resistance to sulfuric acid. While SiC filters have excellent chemical and thermomechanical properties, they are weak against thermal shock compared to a cordierite filter, in that a SiC filter cannot be manufactured in one piece but it must be assembled in segmentations. It should be noted that the relatively large pore size and the poor soot trap mechanism of current filter substrates cause uncontrolled emission of nano-sized PM during a cold start and during regeneration. In contrast, the acicular grain morphology of Si_3N_4 ceramics[16,17] enables them to trap nano-sized PM at the junction site, through a process known as a slit phenomenon, without a significant pressure drop. In addition, Si_3N_4 ceramics have been shown to offer high thermal shock resistance and superior mechanical/chemical stability at high temperatures, which are strongly required properties for a DPF application.

In this research, metal silicon powder, which is less expensive than Si_3N_4 powder, was selected as a starting material, and a reaction-bonding process followed by post sintering was employed to produce a porous Si_3N_4 filter substrate. An unusual and attractive feature of the RBSN fabrication route is that very little change in the size occurs in the compact during nitridation, and close tolerances (approximately 0.1%) on the dimension of a finished component can readily be maintained.[18-20] To aid in the nitridation of metal silicon and the development of a porous microstructure consisting of acicular β-Si_3N_4 grains, a small concentration of a nitriding agent, a pore former and sintering additives were mixed with the silicon powder before the nitriding process. Doping of the nitriding agent drastically accelerates the conversion of silicon into silicon nitride due to the deoxidation of SiO_2 surface layer on silicon particles.[18]

Based on the typical intermingled columnar microstructure of Si_3N_4 ceramics, the goal of this research was to develop a filter substrate exerting the maximum permeability and soot trap performance simultaneously. Emphasis was placed on the relationship between the nitridation rate and various additives, as well on as the characteristics of RBSN and of SRBSN.

2. Experimental Procedure

The metal silicon powder used for the present study was commercially available. Various combinations of sintering additives, a pore former, and a nitriding agent (Fe) were investigated to elucidate a specific effect of any components separately. These are given in Table 1. As the suggested compositions for sintering additives and the nitriding agent were developed for Si_3N_4, the weight percentages used for all additives were based upon Si_3N_4 and not on Si. The required amount of Fe for the experimental trials were obtained from the decomposition of $Fe(NO_3)_3 9H_2O$ into Fe at an elevated temperature.

Approximately 50 g of powder mixtures for each of the compositions were thoroughly milled in a nylon jar with Si_3N_4 balls and ethanol as milling media for 1 h. After the powder mixtures were dried using an evaporator, they were sieved to a particle size <150 μm. The resulting powder mixtures were uniaxially pressed into rectangular pallets measuring 10×10×1.3 mm, and subsequently CIPed at 200 MPa. After shaping, the samples were heated in a nitrogen atmosphere at temperatures ranging from 1250°C to 1450°C, at which reaction-bonding occurs. A maximum of eight specimens from the trials were placed upon a suspended BN-coated graphite plate inside a horizontal tube furnace. The specimens were erected upright on their edges fitting in a small hole on the graphite plate, so that they would be free from contamination and any temperature gradient owing to the contact between specimens and graphite plate. The percent of nitridation was calculated from the weight change before and after the nitriding process. In preparation for the post sintering of the as-nitrided specimen (RBSN), the samples taken from the nitriding furnace were placed upon a BN-coated graphite crucible packed with Si_3N_4 powder filling its volume. Sintering was carried out in a graphite resistance furnace at temperatures between 1600°C and 1800°C, under a nitrogen gas pressure of 0.92 MPa.

SEM (Jeol, JSM-6700F, Japan) was used to observe the fracture surfaces, and X-ray diffraction (Rigaku, D/Max 2200, Japan) and EDX were performed for the phase identification.

3. Results and Discussion

An EDX analysis was conducted to verify the coating mode of the nitriding agent on the silicon powder. Its result is shown in Fig. 1 with the particle image. As the blended nitriding agent can deteriorate the plasticity of the extrud-

Table 1. Investigation of Various Compositions unit : gram

Specimen	Si	Y_2O_3	Al_2O_3	PEG	Fe	β-seed	Pore former
AoPx (w/o pore former)	100	9.7	2.7	3	2	10	-
AoPo (standard)	100	9.7	2.7	3	2	10	20
AxPo (w/o additive)	100	-	-	3	2	10	20

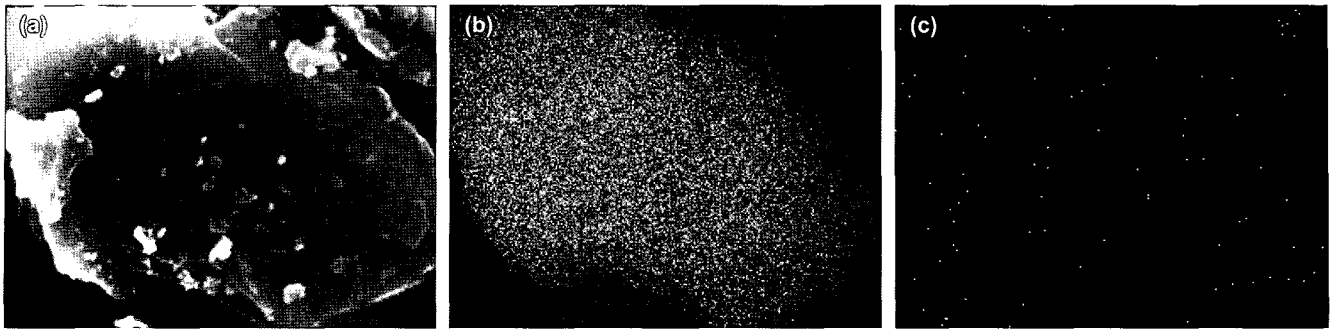

Fig. 1. EDX analysis for the identification of Fe distribution: (a) image of Si particle, (b) detected as Si, and (c) detected as Fe.

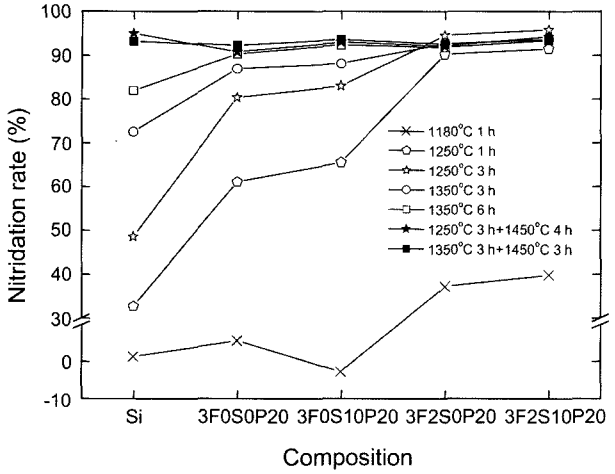

Fig. 2. Nitridation rate of AoPo (standard) specimens.

ing dough and the thermo-mechanical properties of the sintered body, its usage should be limited to the lowest possible. Therefore, the idealistic pattern of the existence of the nitriding agent is believed to be a homogeneous dot coating, as achieved in this experiment. A quantitative analysis yielded a slightly larger doping level than that of the amount actually added, which is ascribed to the intrinsic Fe impurity in the raw silicon powder.

Variations in the nitridation rate with the composition, nitriding temperatures and time for the AoPo (standard) specimens are summarized in Fig. 2. Contrary to the nearly zero rate of the Fe-free specimens (F0S0P20, F0S10P20), approximately 40% of the rate was measured for the Fe-doped specimens (F2S0P20, F2S10P20) at 1180°C, which is a lower temperature than that of the Si-Fe eutectic (1207°C). Nitridation saturates in the 1250°C-3 h set. Increase in both temperature and time from the saturation condition resulted in a decreased nitridation rate for the Fe-doped specimens. As the nitridation rate is calculated from the weight change during the reaction, the decrease in the rate is attributed to weight loss caused by the evaporation of the liquid phase formed between the sintering additives and the nitriding agent. On the other hand, a rate of 80% was found in the 1250°C-3 h set, and saturated nitridation is obtained for a higher temperature and additional time for the 1350°C-6 h set for the Fe-free specimens. In the figure, the Si on the left denotes the data of the dummy silicon compacts used as an oxygen getter.[21] Inversion on the nitridation rate is manifest between the Fe-doped and Fe-free specimens at elevated temperatures, which supports the explanation that the formation of a liquid phase blocks the voidage in compact which hinders the access of the nitriding gas. As reported previously, a slightly enhanced nitridation rate is seen in seeded specimens (F0S10P20, F2S10P20) due to the increased nitriding gas passage by the reaction-uninvolved seed particles.[22] The saturation condition of the nitriding reaction was also confirmed through an XRD analysis when no peaks were detected, indicating unreacted raw silicon. In addition, a higher β-Si_3N_4 content in the Fe-doped specimens agrees well with past research claiming a dominant formation of β-Si_3N_4 by a liquid phase reaction.[18]

The microstructures of both RBSN of the 1250°C-3 h set and subsequently post sintered at 1450°C for 3 h are shown in Fig. 3. A typical microstructure constructed with fine grains and needles is observed for RBSN (a), (b). Both grains and pores have grown substantially by post sintering (c), (d). Compared with the rounded grain morphology for the Fe-free specimen (c), that of the Fe-doped specimen (d) is characterized as having an angular shape, which is typical in a β-Si_3N_4 phase. These observations are well matched with the phase distribution showing a higher β-phase content in both the RBSN and SRBSN of Fe-doped specimens.

Analyzing Fig. 4, the effects of compositional variables, such as sintering additives, the pore former, and the nitriding agent on the nitriding behavior can be stated by combining the phenomena taking place both at a low temperature, (a) 1250°C, and at a high temperature, (b) 1350°C. For the low temperature regime plotted in Fig. 4(a): 1) It is clear that the reactions are promoted by the nitriding agent regardless of the other variables. 2) The lowest nitridation rate in the AoPx (without the pore former) specimens resulted from the smallest nitriding gas passage in the compact. 3) Compared with other variables, it was determined that sintering additives have an insignificant role in the nitriding reaction in this regime. For the high temperature regime plotted in Fig. 4(b): 1) For the Fe-free specimens, the AxPo (without additive) specimens resulted in the lowest nitridation rate, while the AoPx specimens yielded a similar

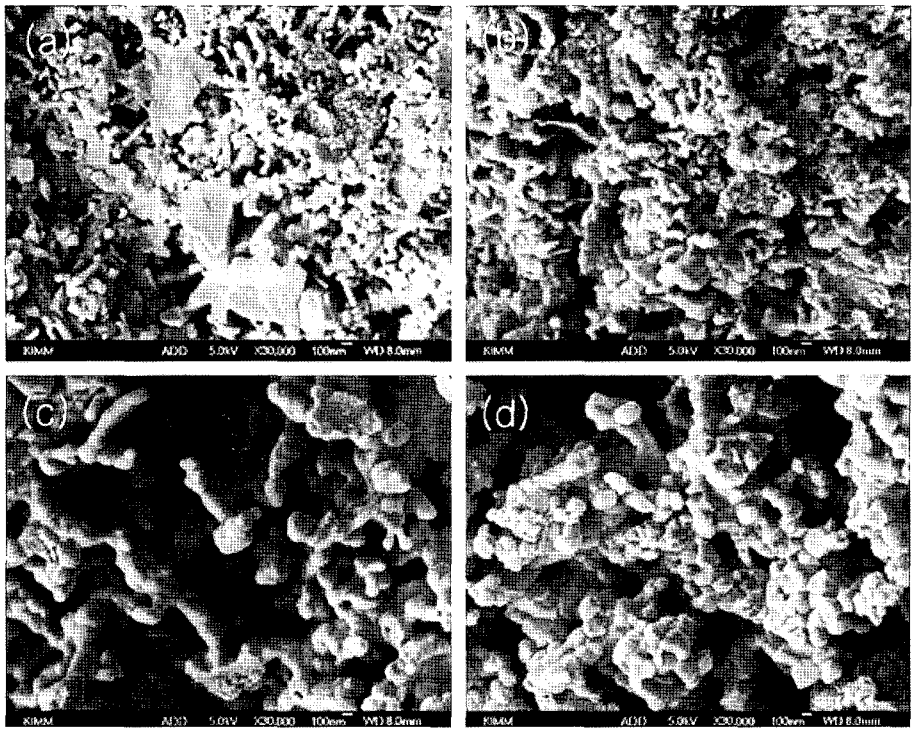

Fig. 3. Fracture morphology of RBSN fabricated at 1250°C for 3 h (a), (b) and SRBSN sintered at 1450°C for 4 h (c), (d) for Fe-free specimen (a), (c) and Fe-doped specimen (b), (d).

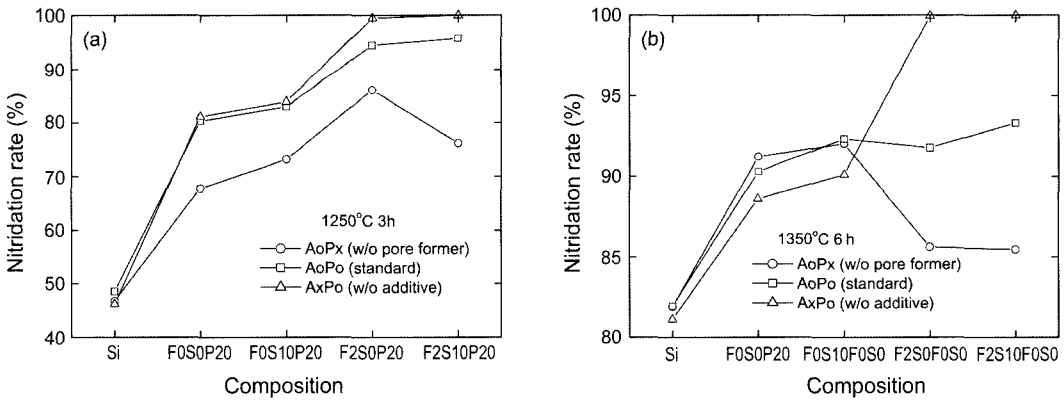

Fig. 4. (a) nitridation rate of 1250°C-3 h set and (b) nitridation rate of 1350°C-6 h set.

value to the AoPo specimens. It is interesting to note that the sintering additives are more effective for accelerating the nitriding reaction in this temperature regime. 2) For the Fe-doped specimens, the rate is highest for AxPo and lowest for AoPx. The negative effect of the nitriding agent was exerted when a liquid phase forms between the sintering additives and the nitriding agent, as mentioned in Fig. 2. It is known that sintering additives react with a SiO_2 layer on silicon powder in a solid state to expose the underling silicon, and eventually promote a nitriding reaction.[23] Thus far, equivocal comments regarding the effect of sintering additives on the nitriding reaction have been reported,[23,24] but it became clear that this depends on the reaction temperature and on other variables such as Fe impurity.

Fig. 5(a) and (b) show the temperature-sorted nitridation rate of the post-sintered specimens originally reaction-bonded at 1250°C and 1350°C, respectively. For RBSN of a low temperature (Fig. 5(a)), the nitridation rate increases as the post sintering temperature increases to 1700°C due to the proceeded nitriding reaction of residual silicon in the RBSN. Past this temperature, it abruptly drops at 1800°C owing to the weight loss derived from the evaporation of the liquid phase at high temperatures. In contrast, the nitridation rates of the specimens reaction-bonded at a high temperature (Fig. 5(b)) are maintained at virtually the same level through the tested post-sintering temperature range. As predicted, the temperature dependency of the porosity, plotted in Fig. 6, for the post-sintered specimens is analo-

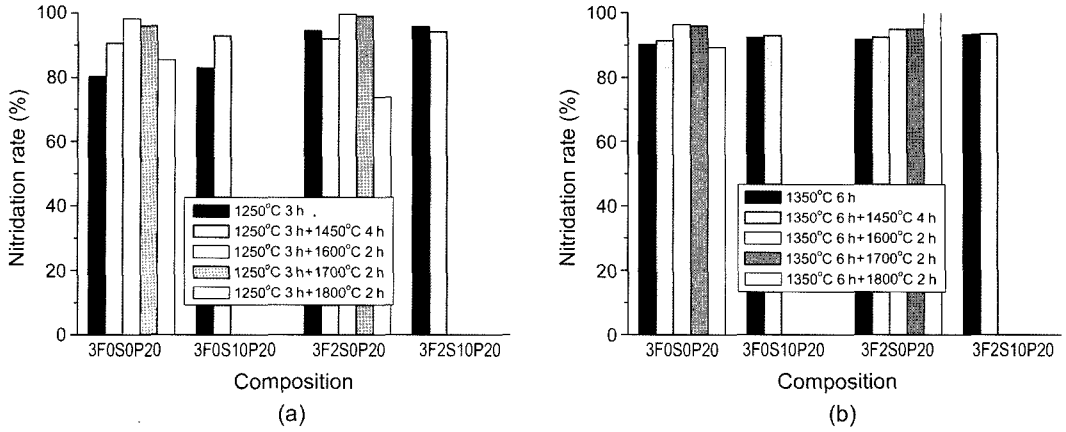

Fig. 5. Nitridation rate of SRBSN using RBSN at (a) 1250°C-3 h set and (b) 1350°C-6 h set.

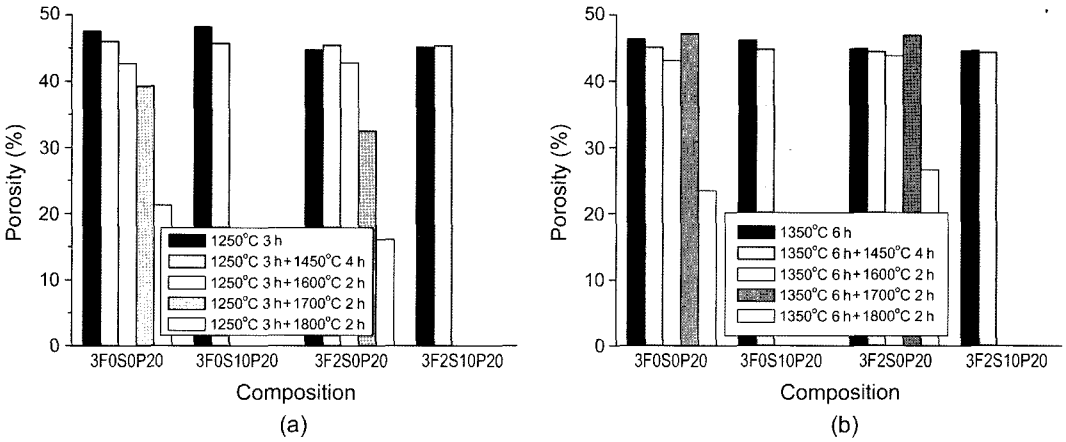

Fig. 6. Porosity of SRBSN using RBSN at (a) 1250°C-3 h set and (b) 1350°C-6 h set.

gous to that of the nitridation rate. With the exception of the large drop that occurred at 1800°C, porosity decreases steadily in a low temperature RBSN, but retains its values in a high temperature RBSN, which is free from residual raw silicon. Similarly, variations in the measured shrinkage accurately resemble those of the porosity. Considering the importance of near-net shape manufacturing with engineering ceramics, high-temperature RBSN followed by post-sintering is preferred to minimize any dimensional change. Further-more, a microstructure observation revealed a jump in grain growth between 1700°C and 1800°C, which is detrimental in terms of the mechanical properties. An XRD analysis conducted on the 1700°C specimens identified the precipitation of a liquid phase consuming the 2nd phases, while a substantially diminished appearance of these phases in the 1800°C specimens were observed. By means of both the increased liquid phase content caused by 2nd phase melting and the decreased viscosity at elevated temperatures, abrupt changes in the grain growth, porosity, and shrinkage are brought about at 1800°C. The lack of shrinkage below 1800°C is attributed to impinged fibrous grain growth competing for the rearrangement of grains in the highly porous microstructure.

In general, RBSN has a porosity of approximately 20 vol%, with 80 vol% of the pores of a size less than 0.1 μm.[20] As the porosity of currently adopted filter substrates in a DPF system is apporoximately 45%, and advanced systems target 60% or more, the addition of a pore former is indispensable to secure permeability. As the amount of blended pore former increases, the porosity of the RBSN increases monotonically but the nitridation rate remains nearly constant opon reaching the highest value with a small dose. A certain amount of pore former is needed to help nitriding gas access the compact, and an excess dose beyond what is needed only contributes to an increase in porosity. In spite of the proportional increase in the porosity with the amount of pore former, the original site of decomposed pore former does not remain empty, it is filled with the reaction product Si_3N_4 as shown in Fig. 7. At temperatures below the melting point of silicon, the pores of the silicon compact become filled with needle-like Si_3N_4.[25-28] The continued reaction increases the number and thickness of the needles, which grow together and generate the fine-grained matrix. The steady development of the α-Si_3N_4 mat is responsible for the increase in the mechanical strength of RBSN. As the pore former site is loosely filled, as shown in the microstructure, there remains

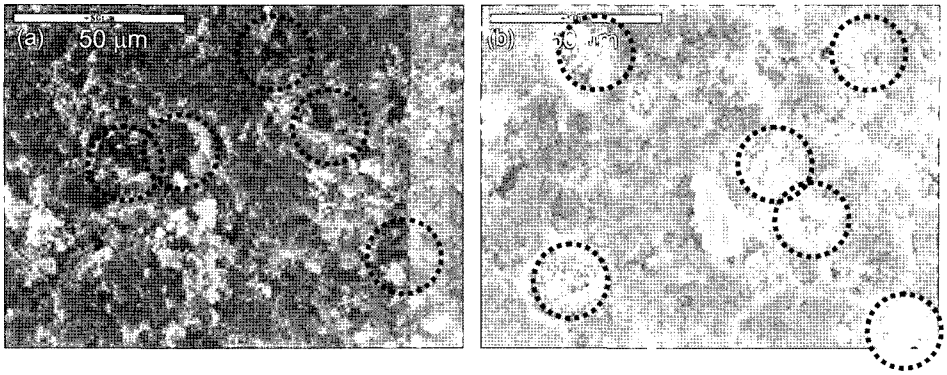

Fig. 7. Fracture morphology showing pore filling by reaction product, Si_3N_4, (a) 1250°C-1 h and (b) 1250°C-3 h.

sufficient space for elongated grains to grow without large amount of impingement. This is why the porosity remains proportional to the addition of pore former filled during the reaction-bonding process.

4. Conclusions

In order to develop microstructure controlling technology for porous RBSN and SRBSN for a DPF application, systematic studies dealing with compositional and processing variables were conducted. The findings by this research are summarized as follows:

1. Saturated nitridation is obtained in the 1350°C-6 h set for Fe-free specimens and in the 1250°C-3 h set for Fe-doped specimens. While forming a liquid phase between the sintering additives and the nitriding agent at elevated temperatures, the nitriding reaction is retarded by the blocking of the nitriding gas passage.

2. In terms of the nitridation accelerating effect, pore former, which provides an open space by thermal decomposition, dominates at a low temperature regime (<1250°C), and a disruption of the SiO_2 layer by the sintering additives prevails at a high temperature regime (<1350°C). The decomposed pore former sites are loosely filled by needle-like Si_3N_4 grains. Elongated large grains are selectively distributed in the vicinity of the loosely filled pores.

3. The porosity and shrinkage of SRBSN depend on the characteristics of RBSN in such a way that specimens nitrided at a relatively high temperature result in higher porosity and smaller shrinkage.

REFERENCES

1. M. Kitayama, K. Hirao, M. Toriyama, and S. Kanzaki, "Thermal Conductivity of β-Si_3N_4: I, Effects of Various Microstructural Factors," *J. Am. Ceram. Soc.*, **82** [11] 3105-12 (1999).
2. M. Kitayama, K. Hirao, A. Tsuga, K. Watari, M. Toriyama, and S. Kanzaki, "Thermal Conductivity of β-Si_3N_4: II, Effect of Lattice Oxygen," *J. Am. Ceram. Soc.*, **83** [8] 1985-92 (2000).
3. M. Kitayama, K. Hirao, K. Watari, M. Toriyama, and S. Kanzaki, "Thermal Conductivity of β-Si_3N_4: III, Effect of Rare Earth (RE=La, Nd, Gd, Y, Yb, and Sc) Oxide Additive," *J. Am. Ceram. Soc.*, **84** [2] 353-58 (2001).
4. K. Watari, K. Hirao, M. E. Brito, M. Toriyama, and S. Kanzaki, "Hot Isostatic Pressing to Increase Thermal Conductivity of Si_3N_4 Ceramics," *J. Mater. Res.*, **14** [4] 1538-41 (1999).
5. H. Yokota and M. Ibukiyama, "Microstructure Tailoring for High Thermal Conductivity of β-Si_3N_4 Ceramics," *J. Am. Ceram. Soc.*, **86** [1] 197-99 (2003).
6. N. Hirosaki, Y. Okamoto, F. Munakata, and Y. Akimune, "Effect of Seeding on the Thermal Conductivity of Self-Reinforced Silicon Nitride," *J. Eur. Ceram. Soc.*, **19** 2183-87 (1999).
7. C. Kawai and A. Yamakawa, "Effect of Porosity and Microstructure on the Strength of Si_3N_4 : Designed Microstructure for High Strength, High Thermal Shock Resistance, and Facile Machining," *J. Am. Ceram. Soc.*, **80** [10] 2705-08 (1997).
8. J. F. Yang, Z. Y. Deng, and T. Ohji, "Fabrication and Characterization of Porous Silicon Nitride Ceramics Using Yb_2O_3 as Sintering Additive," *J. Eur. Ceram. Soc.*, **23** 371-78 (2003).
9. N. Miyakawa, H. Sato, H. Maeno, and H. Takahashi, "Characteristics of Reaction-Bonded Porous Silicon Nitride Honeycomb for DPF Substrate," *JSAE Review*, **24** 269-76 (2003).
10. C. Kawai and A. Yamakawa, "Network Formation of Si_3N_4 Whiskers for the Preparation of Membrane Filters," *J. Mater. Sci. Lett.*, **17** 873-75 (1998).
11. C. Kawai, T. Marsuura, and A. Yamakawa, "Separation-permeation Performance of Porous Si_3N_4 Ceramics Composed of β-Si_3N_4 Grains as Membrane Filters for Microfilteration," *J. Mater. Sci.*, **34** 893-96 (2001).
12. J. F. Yang, G. J. Zhang, and T. Ohji, "Fabrication of Low-shrinkage, Porous Silicon Nitride Ceramics by Addition of a Small Amount of Carbon," *J. Am. Ceram. Soc.*, **84** [7] 1639-41 (2001).
13. J. S. Haggerty and A. Lightfoot, "Opportunities for Enhancing the Thermal Conductivities of SiC and Si_3N_4 Ceramics through Improved Processing," *Ceram. Eng. Sci. Proc.*, **16** [4] 475-87 (1995).

14. N. Kondo, Y. Inagaki, Y. Suzuki, and T. Ohji, "Fabrication of Porous Anisotropic Silicon Nitride by Using Partial Sinter-Forging Technique," *Mater. Sci. Eng. A*, **335** 26-31 (2002).
15. Y. Inagaki, N. Kondo, and T. Ohji, "High Performance Porous Silicon Nitrides," *J. Eur. Ceram. Soc.*, **22** 2489-94 (2002).
16. M. Kramer, M. J. Hoffmann, and G. Petzow, "Grain Growth Kinetics of Si_3N_4 During α/β-Transformation," *Acta Metall. Mater.*, **41** [10] 2939-47 (1993).
17. A. J. Pyzik and D. R. Beaman, "Microstructure and Properties of Self-Reinforced Silicon Nitride," *J. Am. Ceram. Soc.*, **76** [11] 2737-44 (1993).
18. A. J. Moulson, "Reaction-Bonded Silicon Nitride : Its Formation and Properties," *J. Mater. Sci.*, **14** 1017-51 (1979).
19. H. M. Jennings, "On Reactions between Silicon and Nitrogen," *J. Mater. Sci.*, **18** 951-67 (1983).
20. G. Ziegler, J. Heinrich, and G. Wotting, "Relationships between Processing, Microstructure and Properties of Dense and Reaction-Bonded Silicon Nitride," *J. Mater. Sci.*, **22** 3041-86 (1987).
21. D. R. Messier and P. Wong, "Kinetics of Nitridation of Si Powder Compacts," *J. Am. Ceram. Soc.*, **56** [9] 480-85 (1973).
22. S. Y. Lee, K. Amoako-Appiagyei, and H. D. Kim, "Effect of β-Si_3N_4 Seed Crystal on the Microstructure and Mechanical Properties of Sintered Reaction-Bonded Silicon Nitride," *J. Mater. Res.*, **14** [1] 178-84 (1999).
23. H. J. Kleebe and G. Ziegler, "Influence of Crystalline Second Phases on the Densification Behavior of Reaction-bonded Silicon Nitride During Post Sintering under Increased Nitrogen Pressure," *J. Am. Ceram. Soc.*, **72** [12] 2314-17 (1989).
24. N. L. Parr, R. Sands, P. L. Pratt, E. R. W. May, C. R. Shakespeare, and D. S. Thompson, "Structural Aspects of Silicon Nitride," *Powder Met.*, **8** 152-63 (1961).
25. H. M. Jennings and M. H. Richman, "Structure, Formation Mechanisms, and Kinetics of Reaction-Bonded Silicon Nitride," *J. Mater. Sci.*, **11** 2087-98 (1976).
26. H. M. Jennings, S. C. Danforth, and M. H. Richman, "Microstructural Analysis of Reaction-Bonded Silicon Nitride," *Metallaography*, **9** [5] 427-46 (1976).
27. A. Atkinson, P. J. Leatt, A. J. Moulson, and E. W. Roberts, "A Mechanism for the Nitridation of Silicon Powder Compacts," *J. Mater. Sci.*, **9** 981-84 (1974).
28. B. T. Lee and H. D. Kim, "Nitridation Mechanism of Si Compacts Studied by Transmission Electron Microscopy," *Mater. Trans. JIM*, **37** [10] 1547-53 (1996).